

Figure S1. Boxplots of the annual mean, winter (December-January-February: DJF), spring (March-April-May: MAM), summer (June-July-August: JJA), and autumn (September-October-November: SON) sensitivities of precipitation (PR_S), temperature (TA_S), specific humidity (SH_S) and wind speed (WS_S) to solar radiation changes for the 115 sites selected for T&C simulations under SR_{sc} scenario.

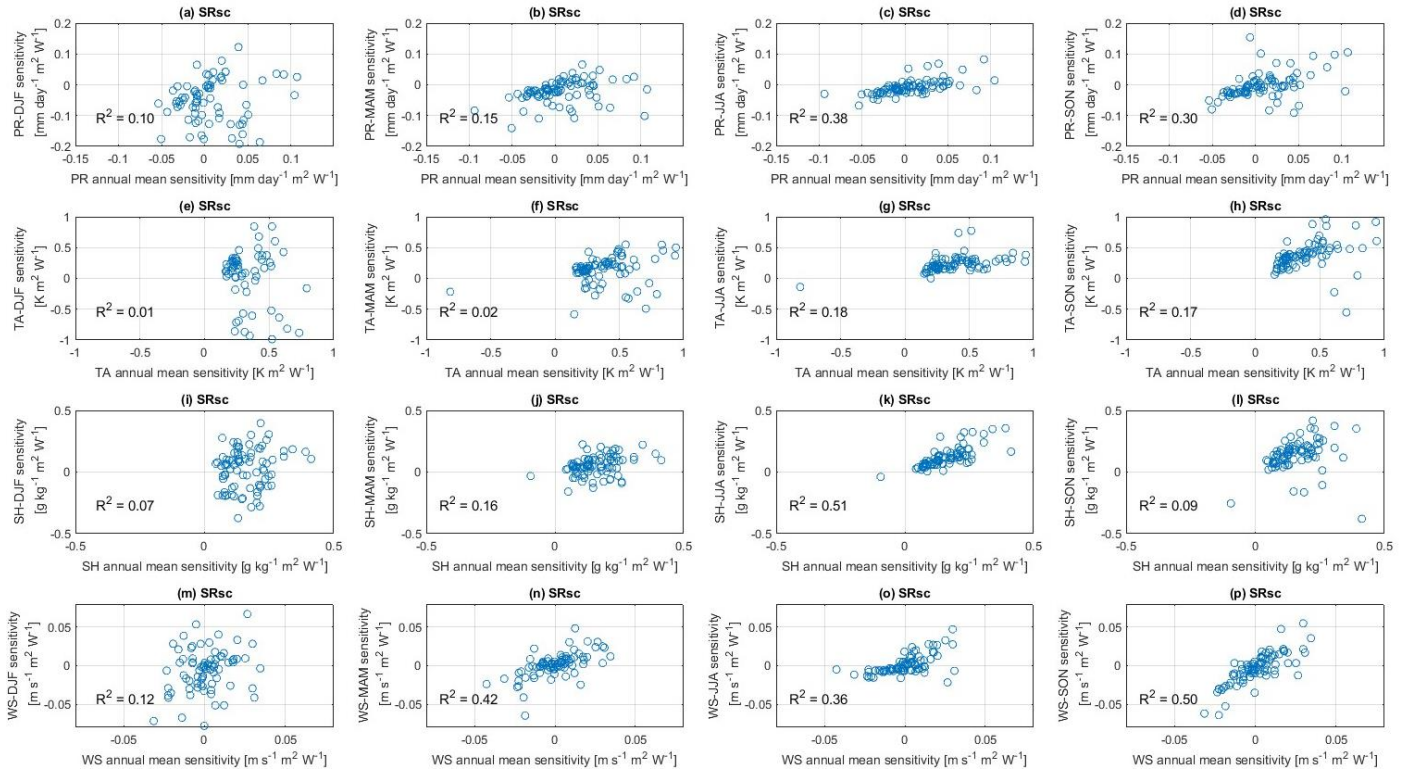


Figure S2. Correlation between the winter (December-January-February: DJF), spring (March-April-May: MAM), summer (June-July-August: JJA), and autumn (September-October-November: SON) sensitivities and annual mean sensitivities of precipitation (PR), temperature (TA), specific humidity (SH) and wind speed (WS) to solar radiation changes for the 115 sites selected for T&C simulations under SR_{sc} scenario. R² is the coefficient of determination associated with the linear regression between seasonal sensitivities and annual mean sensitivities.

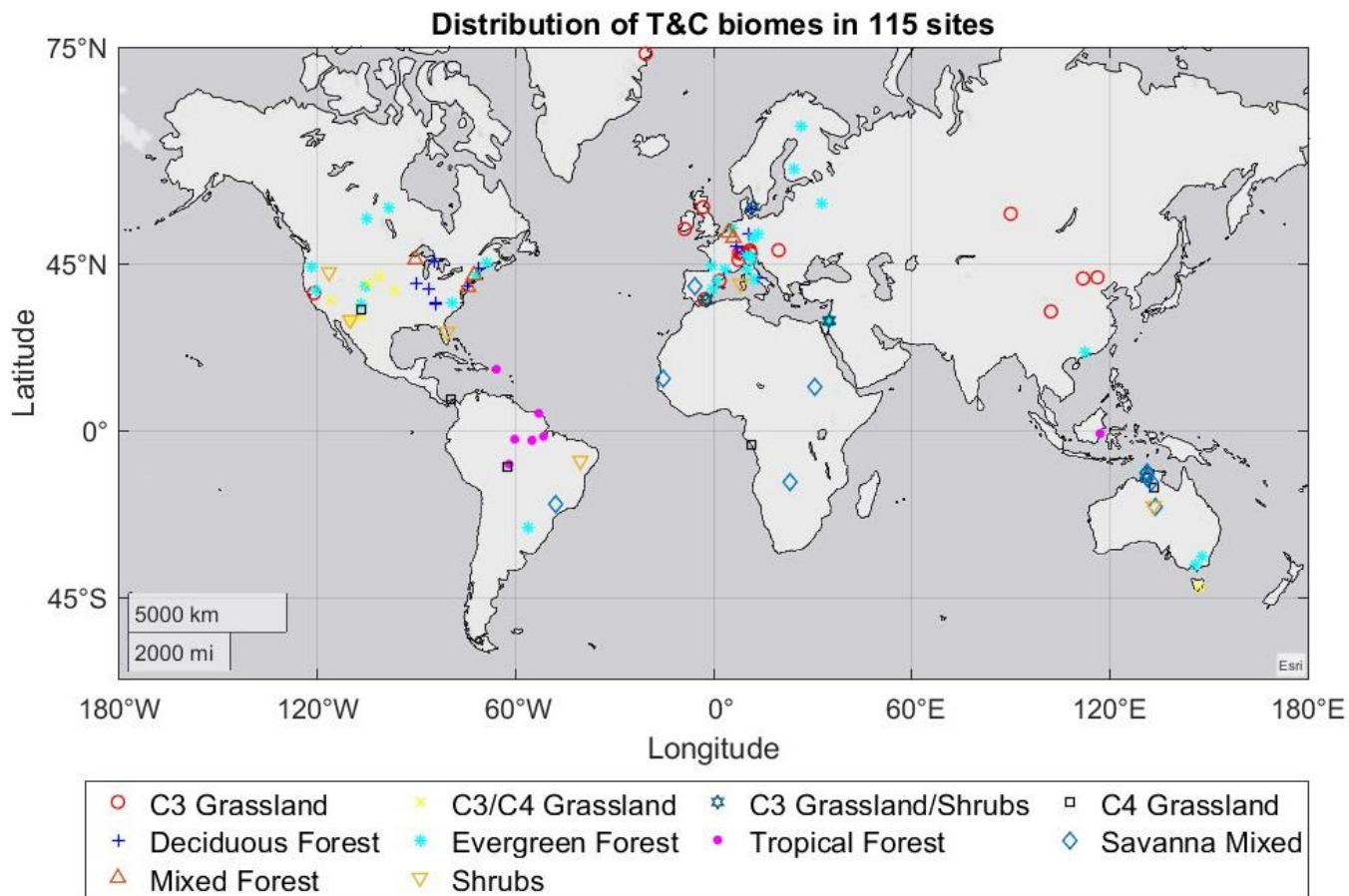


Figure S3. Geographical distribution of the 115 sites used for the ecohydrological T&C simulations and their associated biomes. This map is generated by MATLAB.

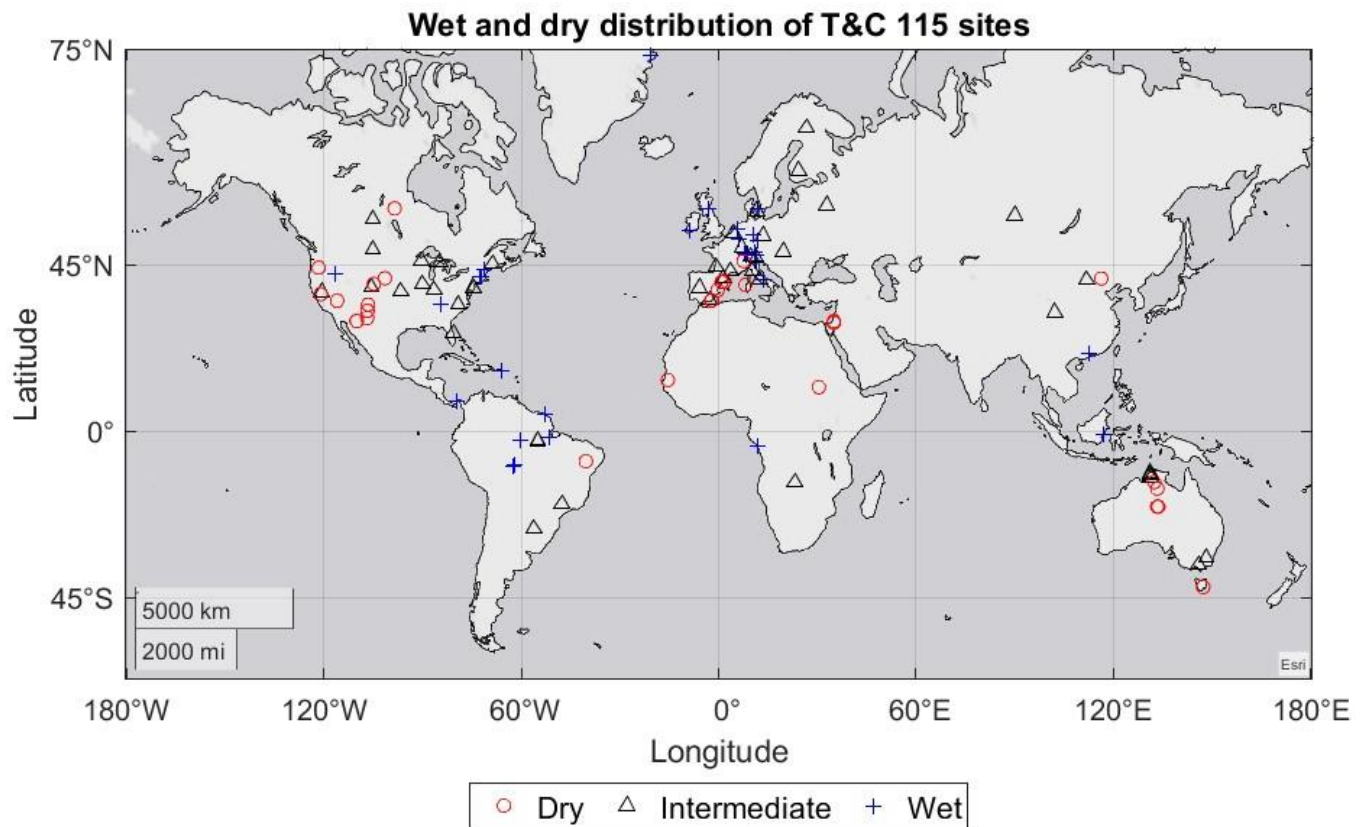


Figure S4. Geographical distribution of the 115 sites used for the ecohydrological T&C simulations and their associated Wetness Index (WI) distribution subdivided in wet, intermediate, and dry sites.

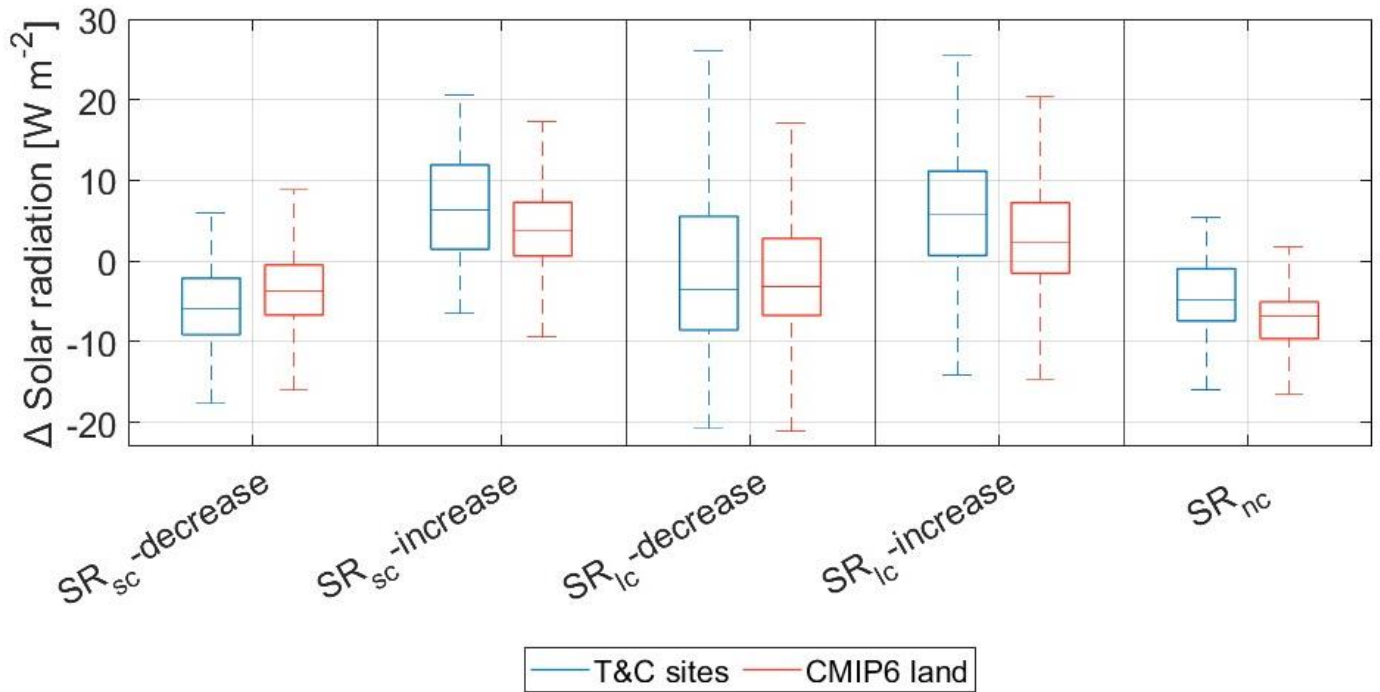


Figure S5. Boxplots of the distribution of changes in solar radiation for the 115 sites selected for T&C simulations (blue boxes) and total land cover in the CMIP6 simulations (red boxes) under the five different scenarios (no climate feedback, short land-atmosphere and long-term climate feedback with increasing and decreasing shortwave radiation).

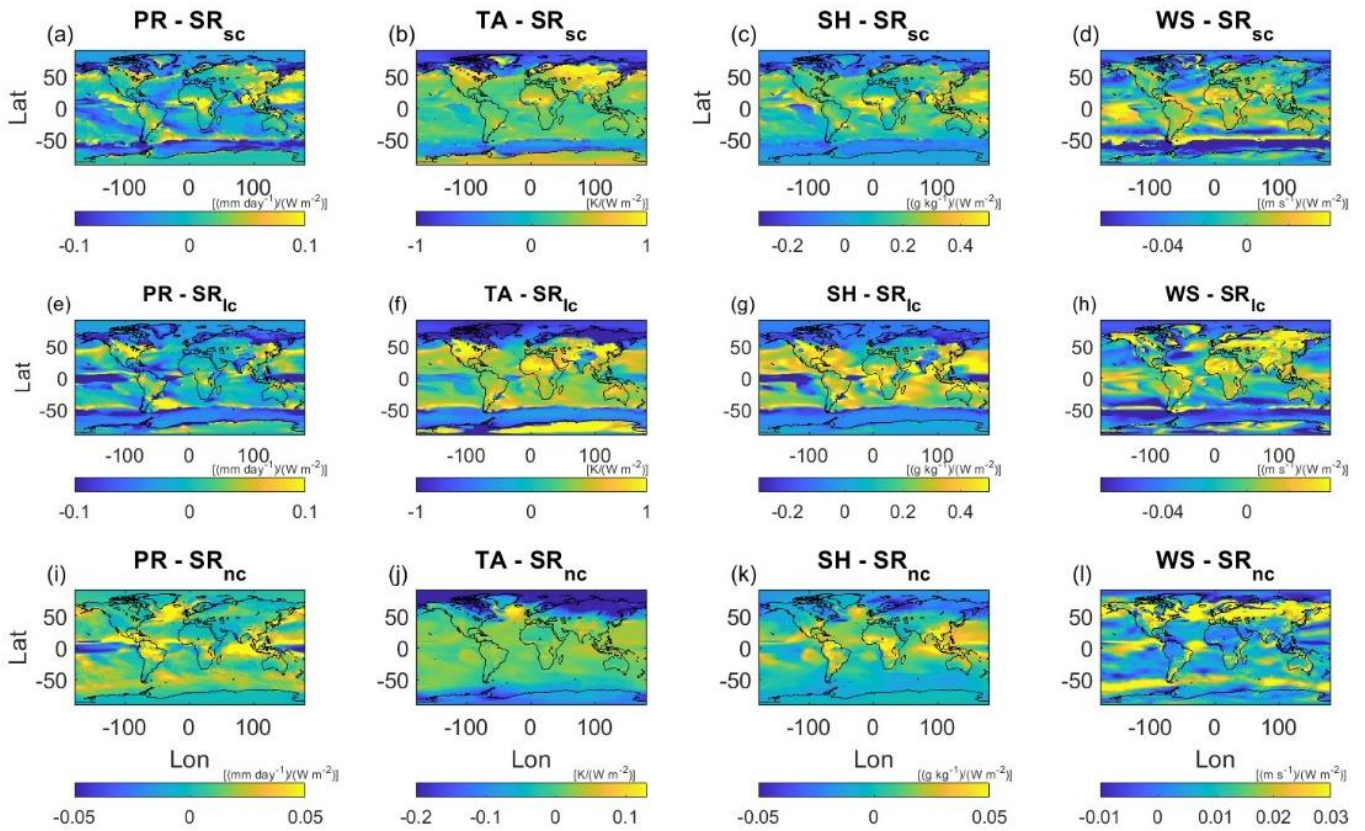


Figure S6. The global spatial pattern of climatic sensitivity to surface solar radiation for precipitation (a, e, i), near surface air temperature (b, f, j), near surface specific humidity (c, g, k), and near surface wind speed (d, h, l) computed for SR_{sc} (a,b,c,d), SR_{ic} (e,f,g,h) and the SR_{nc} (i,j,k,l) scenario.

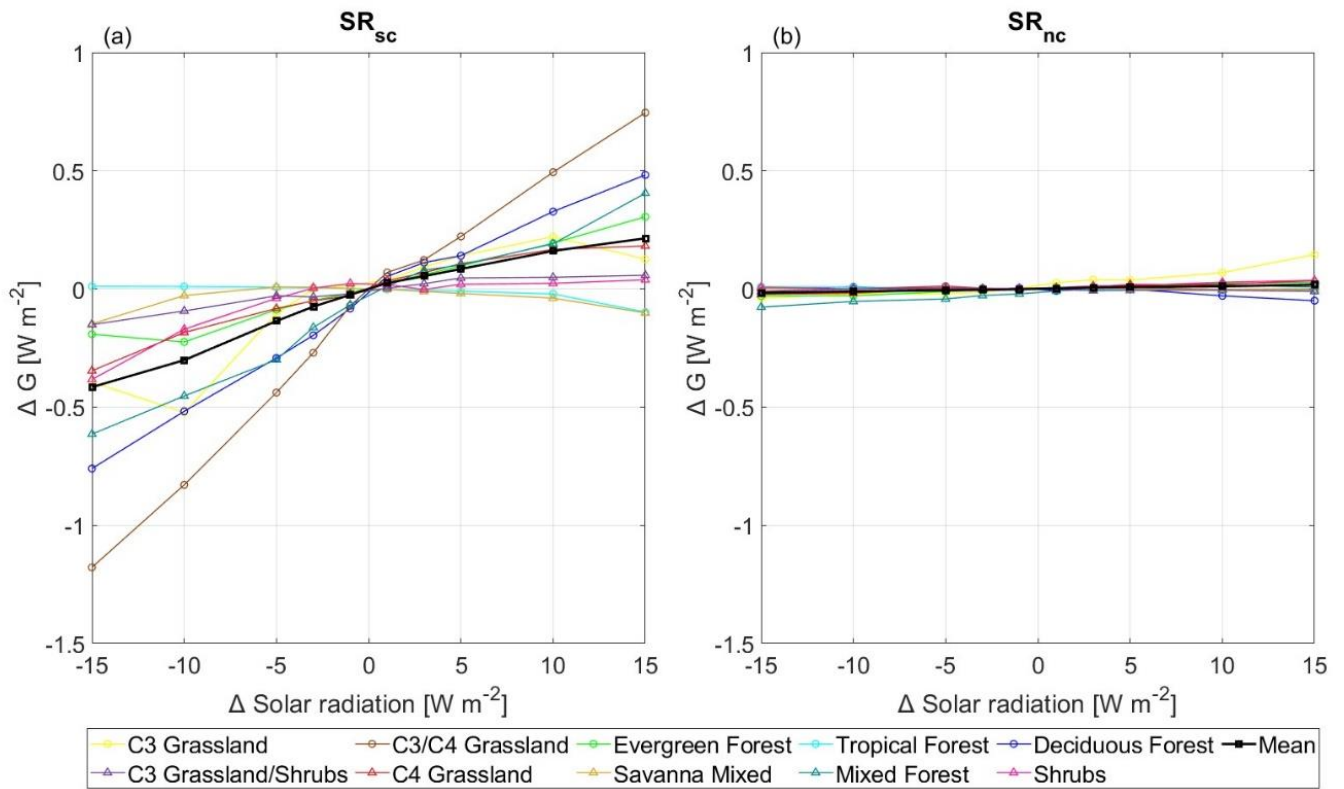


Figure S7. Changes in ground heat flux due to changes in surface solar radiation at the 115 sites simulated with T&C under the (a) SR_{sc} and (b) SR_{nc} scenarios. Colored lines indicate changes in ten different biomes, and thick black lines indicate the average.

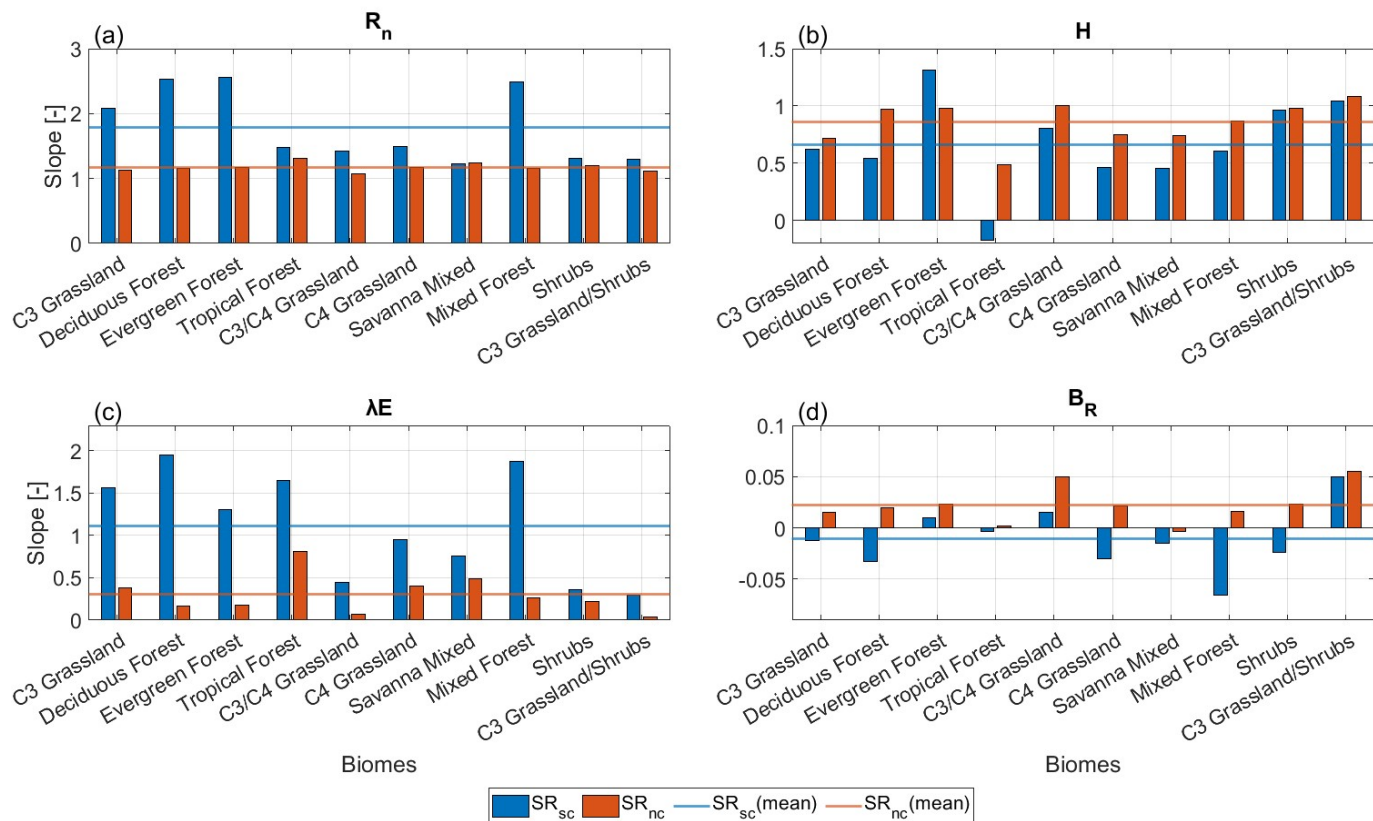


Figure S8. Sensitivities to solar radiation changes of (a) net radiation, (b) sensible heat, (c) latent heat and (d) Bowen ratio across the different biomes in the SR_{sc} and SR_{nc} scenarios. The reference line indicates the average. These sensitivities are computed as the slopes of the linear regression between changes in a given variable and changes in short-wave solar radiation from -5 W m^{-2} to 5 W m^{-2} .

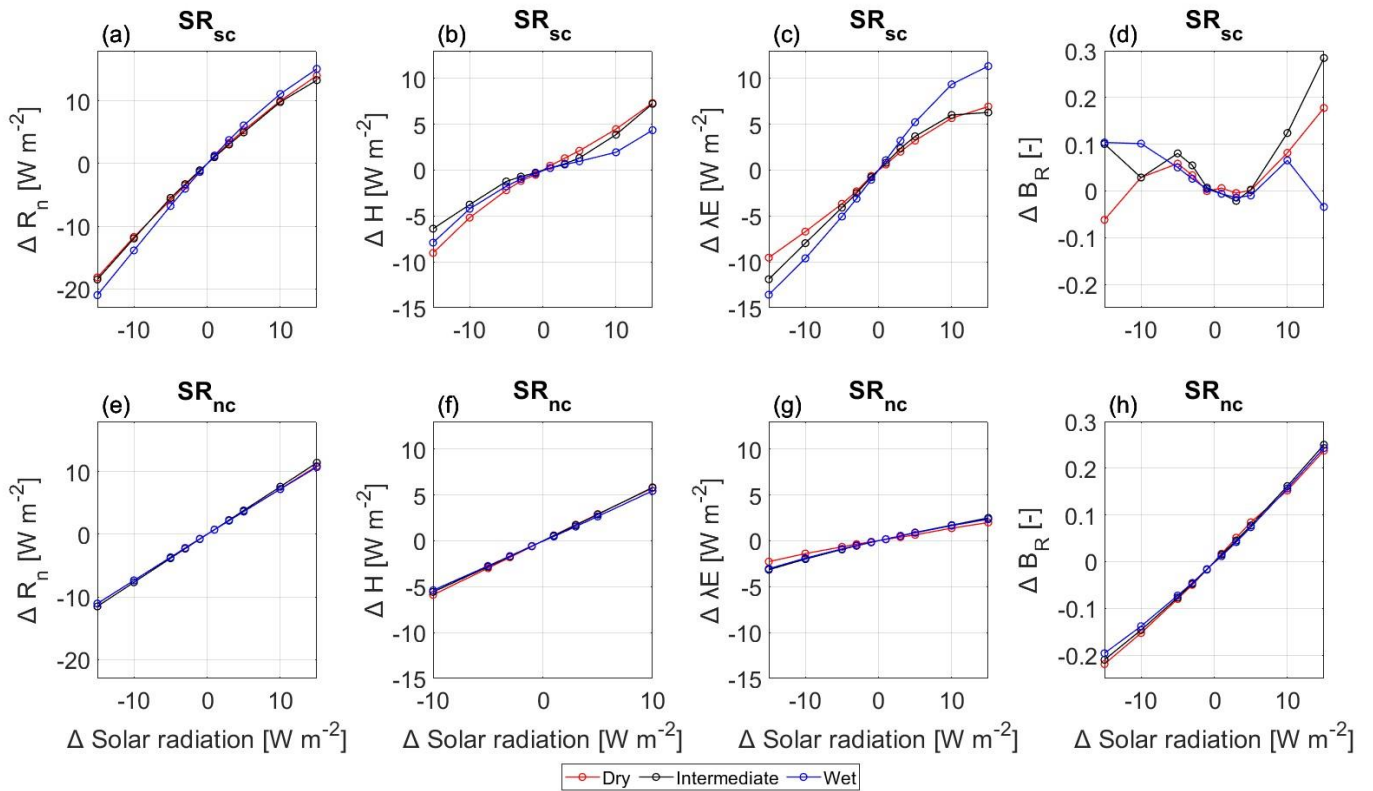


Figure S9. Changes in the energy fluxes (a) (e) net radiation, (b) (f) sensible heat, (c) (g) latent heat, and (d) (h) Bowen ratio due to changing surface solar radiation at the 115 sites simulated with T&C for the SR_{sc} and SR_{nc} scenarios. Colored lines indicate changes for dry, intermediate and wet conditions as expressed by the Wetness Index.

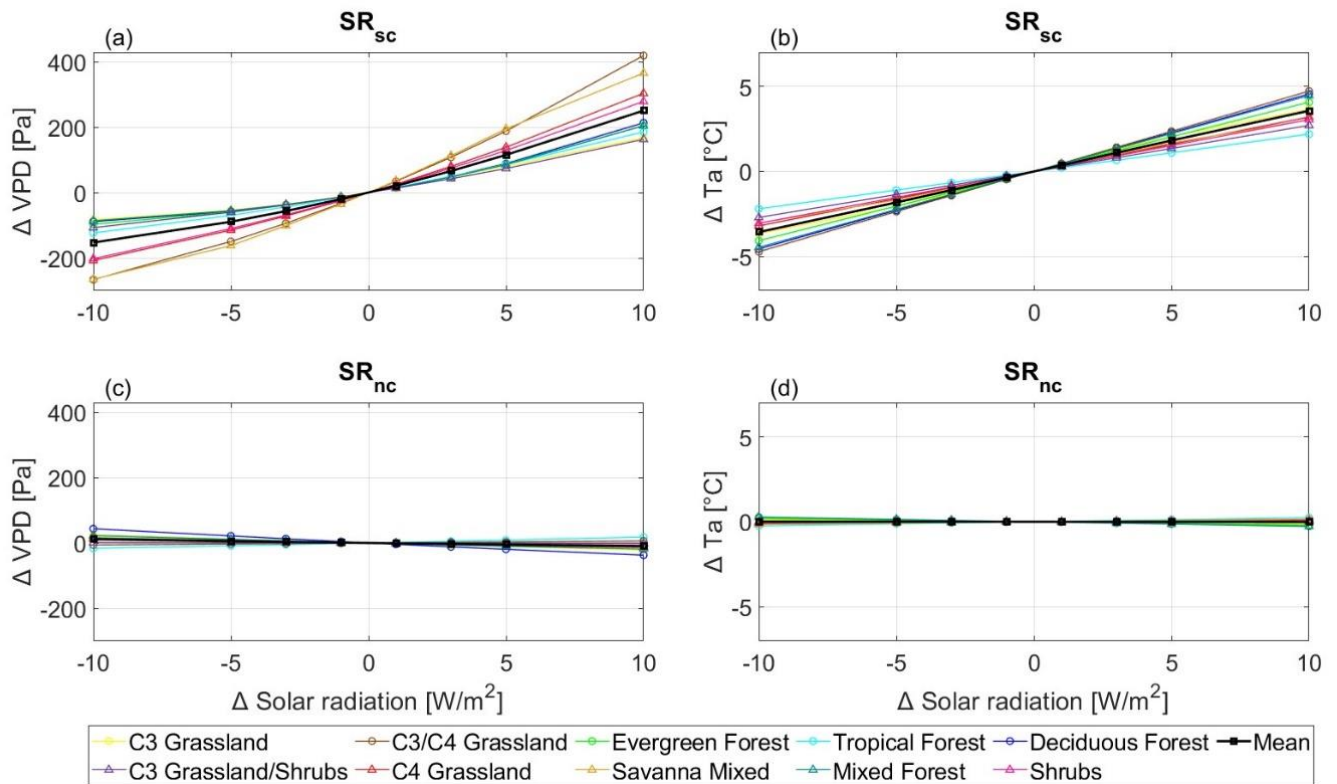


Figure S10. Changes in (a) (c) VPD and (b) (d) air temperature due to changes in surface solar radiation at the 115 sites simulated with T&C under the SR_{sc} and SR_{nc} scenarios. Colored lines indicate changes in ten different biomes, and thick black lines indicate averages.

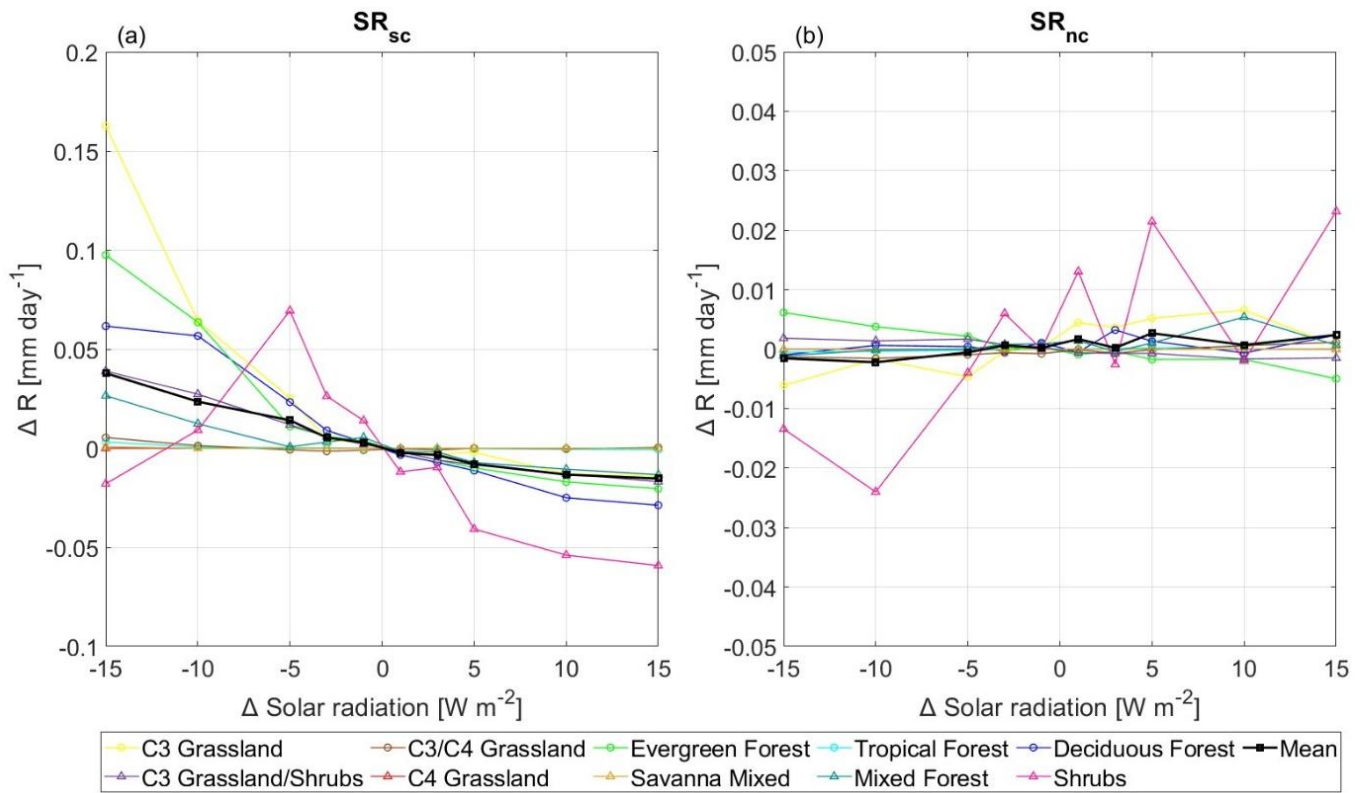


Figure S11. Changes in surface runoff due to changes in surface solar radiation at the 115 sites simulated with T&C under the (a) SR_{sc} and (b) SR_{nc} scenarios. Colored lines indicate changes in ten different biomes, and thick black lines indicate the average.

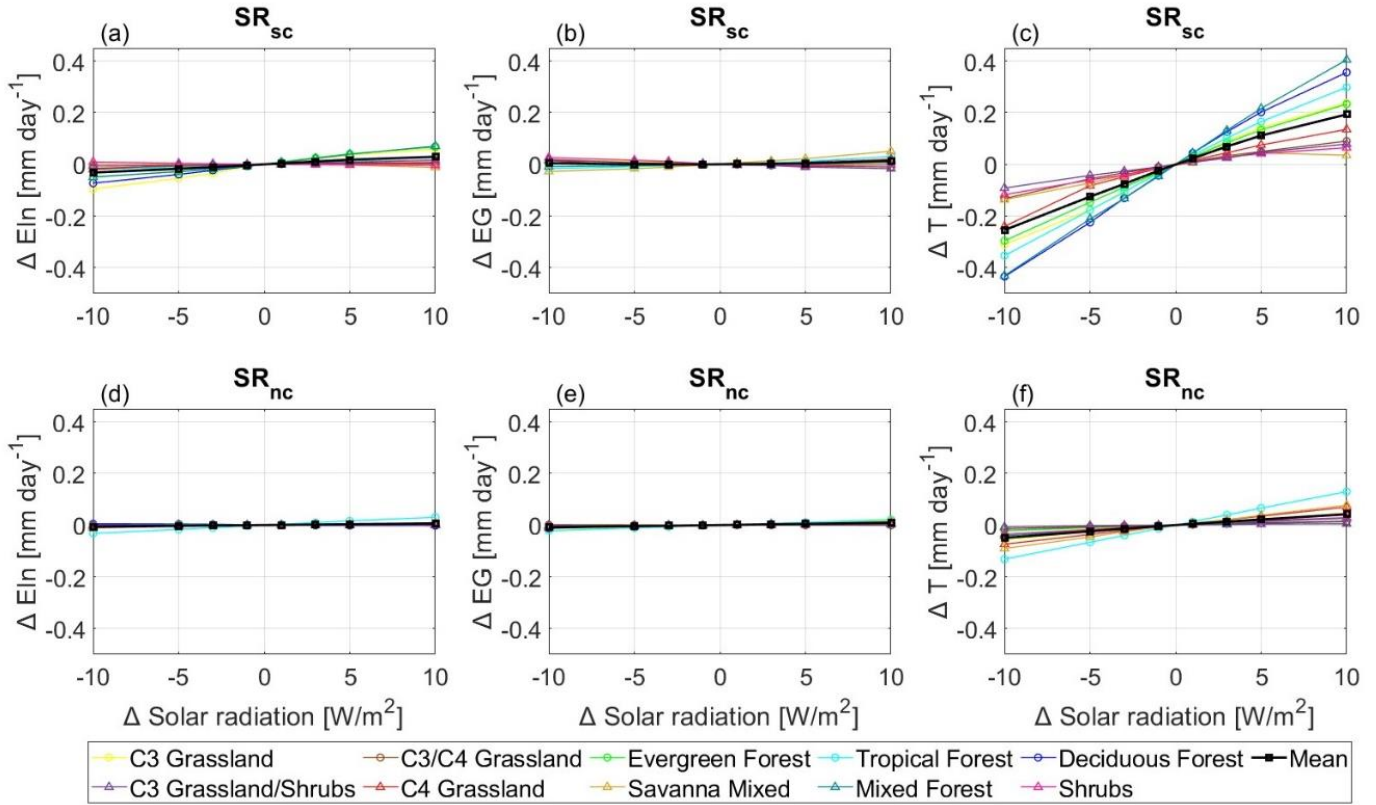


Figure S12. Changes in (a) (d) evaporation from interception, (b) ground evaporation, and (c) (f) transpiration driven by changes in surface solar radiation at the 115 sites simulated with T&C under the SR_{sc} and SR_{nc} scenarios. Colored lines indicate changes in ten different biomes, and thick black lines indicate the average.

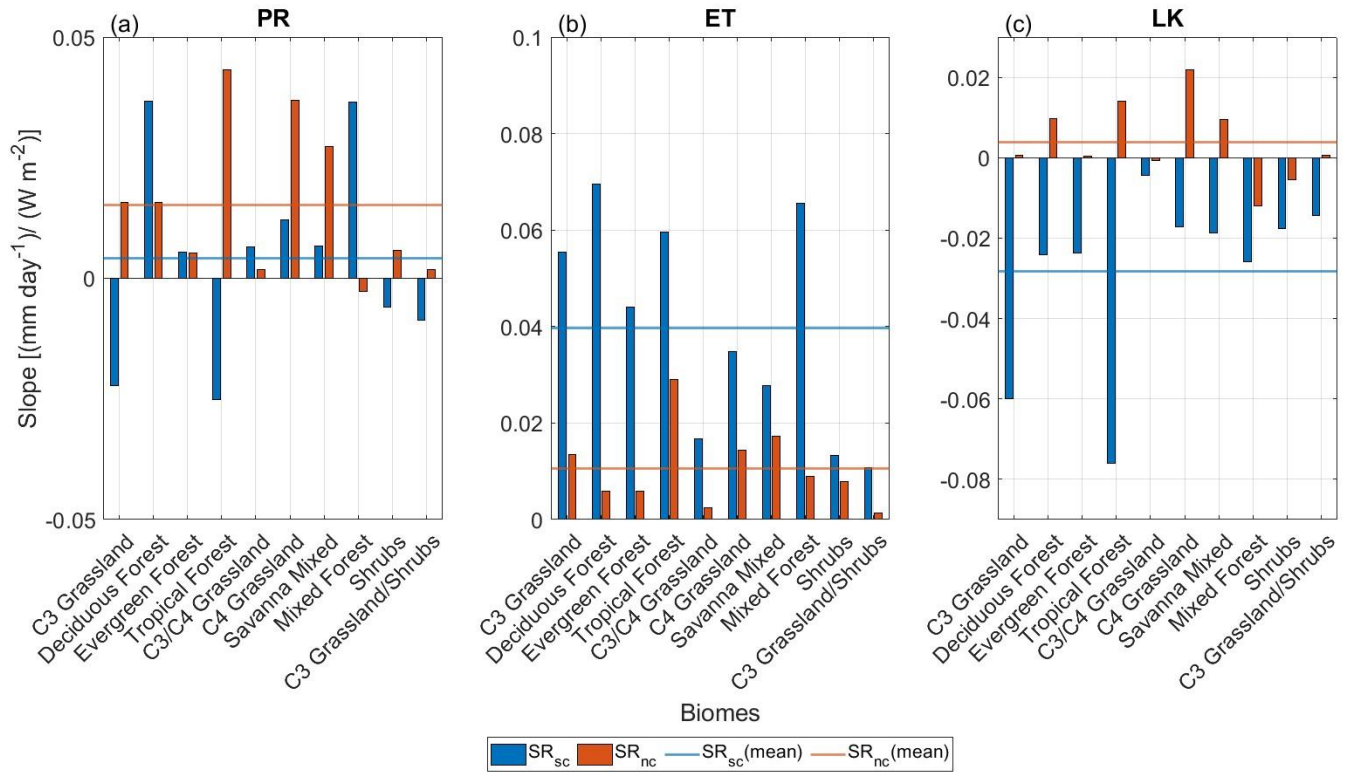


Figure S13. Sensitivity of (a) precipitation, (b) evapotranspiration, (c) and soil leakage to solar radiation changes spanning different biomes under the SR_{sc} and SR_{nc} scenarios. The reference line indicates the average across all sites. These sensitivities are computed as the slopes of the linear regression between changes in hydrological variables and changes in short-wave solar radiation from -5 W m^{-2} to 5 W m^{-2} .

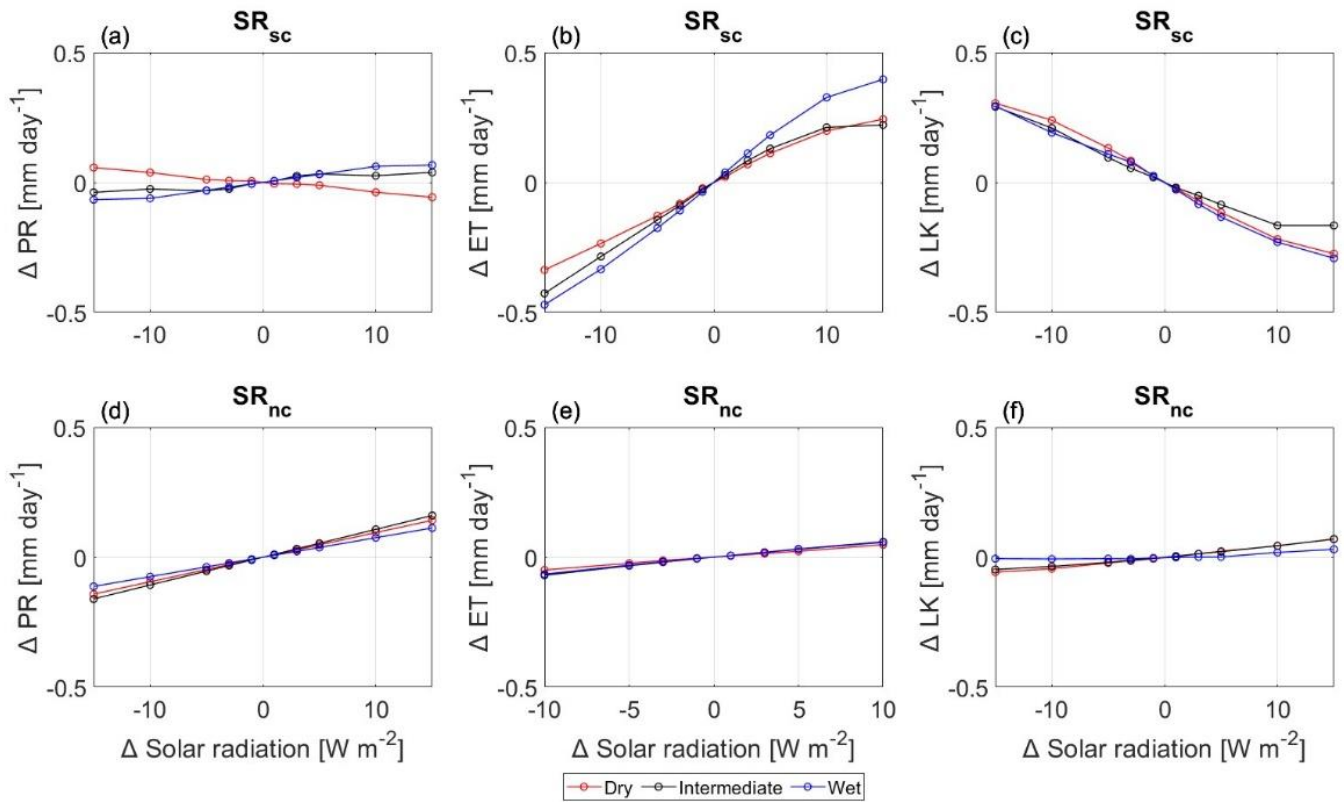


Figure S14. Changes in three hydrological variables (a) (d) precipitation, (b) (e) evapotranspiration, and (c) (f) soil leakage due to changes in surface solar radiation at the 115 sites simulated with T&C under the SR_{sc} and SR_{nc} scenarios. Colored lines indicate changes for dry, intermediate and wet conditions as expressed by the Wetness Index.

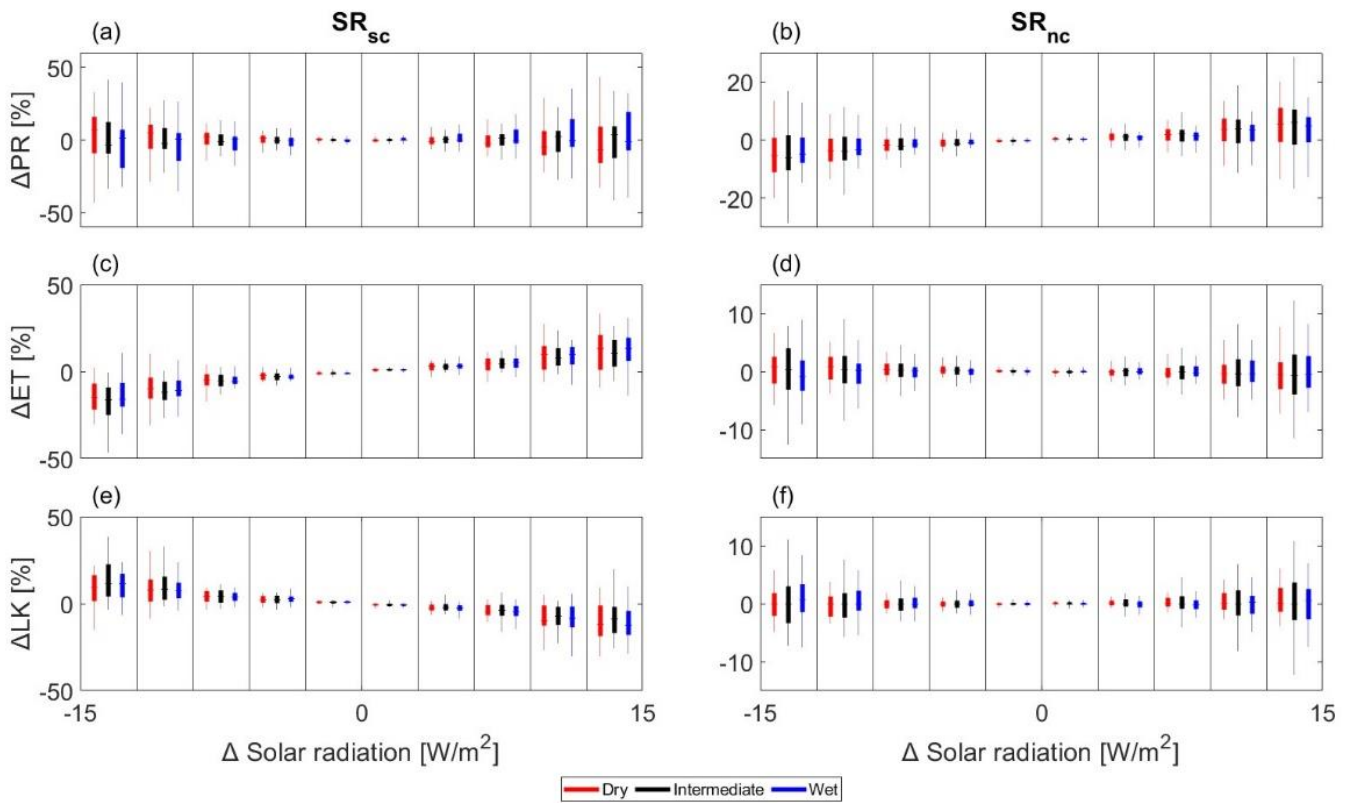


Figure S15. Distributions of relative changes in (a) (b) precipitation, (c) (d) evapotranspiration and (e) (f) leakage under the SR_{sc} and SR_{nc} scenarios, respectively. To avoid non-informative high values, due to extremely low baseline ET and LK, changes in ET and LK were rescaled based on their proportion of PR, for instance a 1% change in the plot is a 1% change on the ET/PR quantity.

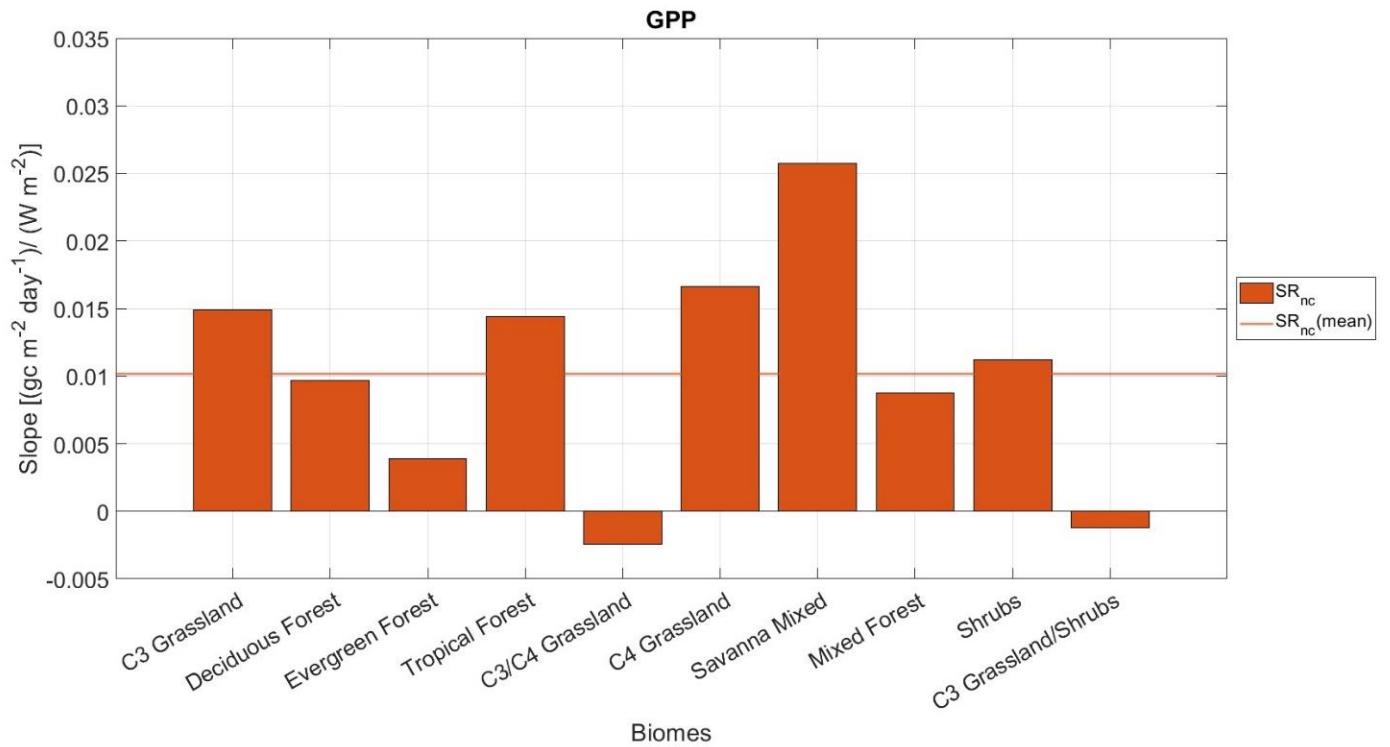


Figure S16. Sensitivity of GPP to solar radiation changes spanning different biomes under SR_{nc} scenario. The reference line indicates the average. These sensitivities are computed as the slopes of the linear regression between changes in GPP and changes in short-wave solar radiation from -5 W m⁻² to 5 W m⁻².

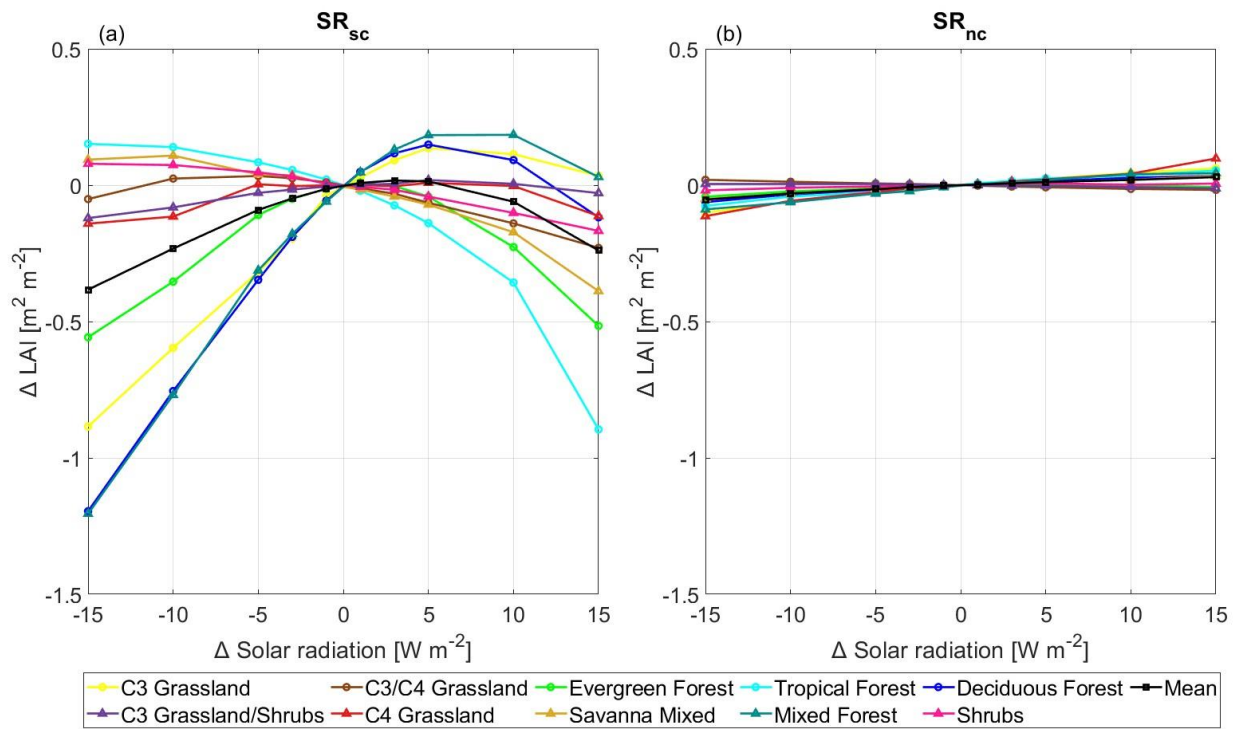


Figure S17. Changes in LAI driven by surface solar radiation changes at 115 sites simulated with T&C under the SR_{sc} and SR_{nc} scenarios. Coloured lines indicate changes in ten different biomes, and thick black lines indicate the average across biomes. The cases with $\Delta PR > \pm 50\%$ have been excluded as outliers.

Model	Reference
IPSL-CM6A-LR	Boucher et al., 2020
CESM2-WACCM	Gettelman et al., 2019
CNRM-ESM2-1	Séférian et al., 2019
MIROC-ES2H	Kawamiya et al., 2020
MRI-ESM2-0	Yukimoto et al., 2019
CESM2	Danabasoglu et al., 2020

Table S1. The supporting references for the six GCM models used in this study.

Table S2. Statistics of the T&C simulation results for the 115 sites. See additional file TableS2.xlsx.

Categories	number of sites
Evergreen Forest	29
C3 Grassland	23
Deciduous Forest	14
Savanna Mixed	10
Tropical Forest	8
C3 / C4 Grassland	8
C4 Grassland	7
Shrubs	6
Mixed Forest	5
C3 Grassland / Shrubs	5
Dry	31
Intermediate	45
Wet	39

Table S3. Classification of 115 T&C sites and the number of locations it covers. The classification for wet/intermediate/dry locations is based on the wetness index: dry (wetness index < 0.5), intermediate (0.5 < wetness index < 1), wet (wetness index > 0.5).

Variables	Scenario	C3	Deciduous Forest	Evergreen	Tropical	C3/C4	C4	Savanna	Mixed	Shrubs	C3	Mean
		Grassland	Grassland/Shrubs	Forest	Forest	Grassland	Grassland	Mixed	Forest		Grassland/Shrubs	
Net radiation [-]	SR _{sc}	2.079	2.525	2.559	1.486	1.429	1.488	1.230	2.485	1.310	1.302	1.789
	SR _{nc}	1.129	1.158	1.170	1.315	1.070	1.177	1.244	1.153	1.200	1.120	1.174
Sensible heat [-]	SR _{sc}	0.625	0.545	1.315	-0.170	0.808	0.461	0.459	0.606	0.961	1.044	0.665
	SR _{nc}	0.720	0.971	0.980	0.489	1.000	0.749	0.745	0.871	0.977	1.079	0.858
Latent heat [-]	SR _{sc}	1.561	1.949	1.303	1.655	0.442	0.953	0.761	1.877	0.361	0.296	1.116
	SR _{nc}	0.386	0.172	0.180	0.816	0.067	0.402	0.486	0.260	0.222	0.039	0.303
Bowen ratio [m ² W ⁻¹]	SR _{sc}	-0.012	-0.033	0.010	-0.004	0.015	-0.030	-0.015	-0.066	-0.024	0.050	-0.011
	SR _{nc}	0.015	0.019	0.023	0.002	0.050	0.021	-0.003	0.016	0.023	0.055	0.022
Precipitation [mm day ⁻¹ m ² W ⁻¹]	SR _{sc}	-0.022	0.037	0.005	-0.025	0.007	0.012	0.007	0.036	-0.006	-0.009	0.004
	SR _{nc}	0.016	0.016	0.005	0.043	0.002	0.037	0.027	-0.003	0.006	0.002	0.015
Evapotranspiration [mm day ⁻¹ m ² W ⁻¹]	SR _{sc}	0.056	0.070	0.044	0.060	0.017	0.035	0.028	0.066	0.013	0.011	0.040
	SR _{nc}	0.013	0.006	0.006	0.029	0.002	0.014	0.017	0.009	0.008	0.001	0.011
Leakage [mm day ⁻¹ m ² W ⁻¹]	SR _{sc}	-0.060	-0.024	-0.024	-0.076	-0.004	-0.017	-0.019	-0.026	-0.018	-0.014	-0.028
	SR _{nc}	0.001	0.010	0.000	0.014	-0.001	0.022	0.009	-0.012	-0.005	0.001	0.004
GPP [gc m ⁻² day ⁻¹ m ² W ⁻¹]	SR _{nc}	0.015	0.010	0.004	0.014	-0.002	0.017	0.026	0.009	0.011	-0.001	0.010

Table S4. Sensitivity of ecohydrological variables to changes in solar radiation across ten biomes. The bold texts indicate the average across all biomes. These sensitivities are computed as the slopes of the linear regression between changes in ecological variables and changes in short-wave solar radiation from -5 W m^{-2} to 5 W m^{-2} .

Categories	Δ GPP [%]			
Scenarios	SR _{sc}	SR _{nc}	SR _{sc}	SR _{nc}
ΔR_{sw} [W m ⁻²]	-5	-5	+5	+5
Evergreen Forest	-7.7	-0.6	4.3	0.2
C3 Grassland	-15.0	-1.7	8.6	1.5
Deciduous Forest	-13.5	-1.1	7.1	1.1
Savanna Mixed	-2.6	-4.1	-4.7	2.1
Tropical Forest	0.6	-1.5	-3.2	1.5
C3 / C4 Grassland	-4.7	0.2	0.2	-0.2
C4 Grassland	0.6	-1.9	1.9	1.7
Shrubs	0.1	-1.1	-1.1	1.3
Mixed Forest	-19.3	-1.3	14.8	0.6
C3 Grassland / Shrubs	-3.6	0.2	3.0	-0.1
Mean	-6.5	-1.3	3.1	1.0

Table S5. The mean percentage change in GPP across 10 biomes under the scenarios with 5 W m⁻² increased/decreased solar radiation.

Variable	Scenario	Changes [%]	
		$\Delta R_{sw} = -5 \text{ W m}^{-2}$	$\Delta R_{sw} = +5 \text{ W m}^{-2}$
Net radiation	SR _{sc}	-6.0	5.4
	SR _{nc}	-4.1	4.1
Sensible heat	SR _{sc}	-3.6	3.0
	SR _{nc}	-6.2	6.2
Latent heat	SR _{sc}	-8.4	8.0
	SR _{nc}	-2.0	1.9
Bowen ratio	SR _{sc}	5.0	-1.0
	SR _{nc}	-8.0	8.0
Precipitation	SR _{sc}	-0.8	0.8
	SR _{nc}	-1.9	1.9
Evapotranspiration	SR _{sc}	-8.4	8.0
	SR _{nc}	-2.0	1.9
Leakage	SR _{sc}	8.9	-9.1
	SR _{nc}	-1.5	1.4
GPP	SR _{sc}	-6.5	3.1
	SR _{nc}	-1.3	1.0

Table S6. The mean percentage change in ecohydrological variables under the scenarios with 5 W m^{-2} increased/decreased solar radiation averaged across all biomes.

Reference

- Boucher, O., Servonnat, J., Albright, A. L., Aumont, O., Balkanski, Y., Bastrikov, V., Bekki, S., Bonnet, R., Bony, S., Bopp, L., Braconnot, P., Brockmann, P., Cadule, P., Caubel, A., Cheruy, F., Codron, F., Cozic, A., Cugnet, D., D'Andrea, F., ... Vuichard, N.: Presentation and Evaluation of the IPSL-CM6A-LR Climate Model. *Journal of Advances in Modeling Earth Systems*, 12(7), e2019MS002010. <https://doi.org/10.1029/2019MS002010>, 2020.
- Danabasoglu, G., Lamarque, J. -F., Bacmeister, J., Bailey, D. A., DuVivier, A. K., Edwards, J., Emmons, L. K., Fasullo, J., Garcia, R., Gettelman, A., Hannay, C., Holland, M. M., Large, W. G., Lauritzen, P. H., Lawrence, D. M., Lenaerts, J. T. M., Lindsay, K., Lipscomb, W. H., Mills, M. J., ... Strand, W. G.: The Community Earth System Model Version 2 (CESM2). *Journal of Advances in Modeling Earth Systems*, 12(2), e2019MS001916. <https://doi.org/10.1029/2019MS001916>, 2020.
- Gettelman, A., Mills, M. J., Kinnison, D. E., Garcia, R. R., Smith, A. K., Marsh, D. R., Tilmes, S., Vitt, F., Bardeen, C. G., McInerney, J., Liu, H. -L., Solomon, S. C., Polvani, L. M., Emmons, L. K., Lamarque, J. -F., Richter, J. H., Glanville, A. S., Bacmeister, J. T., Phillips, A. S., ... Randel, W. J.: The Whole Atmosphere Community Climate Model Version 6 (WACCM6). *Journal of Geophysical Research: Atmospheres*, 124(23), 12380–12403. <https://doi.org/10.1029/2019JD030943>, 2019.
- Kawamiya, M., Hajima, T., Tachiiri, K., Watanabe, S., & Yokohata, T.: Two decades of Earth system modeling with an emphasis on Model for Interdisciplinary Research on Climate (MIROC). *Progress in Earth and Planetary Science*, 7(1), 64. <https://doi.org/10.1186/s40645-020-00369-5>, 2020.
- Séférian, R., Nabat, P., Michou, M., Saint-Martin, D., Voldoire, A., Colin, J., Decharme, B., Delire, C., Berthet, S., Chevallier, M., Sénési, S., Franchisteguy, L., Vial, J., Mallet, M., Joetzjer, E., Geoffroy, O., Guérémy, J., Moine, M., Msadek, R., ... Madec, G.: Evaluation of CNRM Earth System Model, CNRM-ESM2-1: Role of Earth System Processes in Present-Day and Future Climate. *Journal of Advances in Modeling Earth Systems*, 11(12), 4182–4227. <https://doi.org/10.1029/2019MS001791>, 2019.
- Yukimoto, S., Kawai, H., Koshiro, T., Oshima, N., Yoshida, K., Urakawa, S., Tsujino, H., Deushi, M., Tanaka, T., Hosaka, M., Yabu, S., Yoshimura, H., Shindo, E., Mizuta, R., Obata, A., Adachi, Y., & Ishii, M.: The Meteorological Research Institute Earth System Model Version 2.0, MRI-ESM2.0: Description and Basic Evaluation of the Physical Component. *Journal of the Meteorological Society of Japan*. Ser. II, 97(5), 931–965. <https://doi.org/10.2151/jmsj.2019-051>, 2019.